

Measurement of the form-factor ratios for $D^+ \rightarrow \bar{K}^{*0} e^+ \nu_e$

E. M. Aitala,⁹ S. Amato,¹ J. C. Anjos,¹ J. A. Appel,⁵ D. Ashery,¹⁵ S. Banerjee,⁵
I. Bediaga,¹ G. Blaylock,⁸ S. B. Bracker,¹⁶ P. R. Burchat,¹⁴ R. A. Burnstein,⁶ T. Carter,⁵
H. S. Carvalho,¹ N. K. Coptly,¹³ L. M. Cremaldi,⁹ C. Darling,¹⁹ K. Denisenko,⁵
A. Fernandez,¹² G. Fox,¹³ P. Gagnon,² K. Gounder,⁹ A. M. Halling,⁵ G. Herrera,⁴
G. Hurvits,¹⁵ C. James,⁵ P. A. Kasper,⁶ S. Kwan,⁵ D. C. Langs,¹¹ J. Leslie,² B. Lundberg,⁵
S. MayTal-Beck,¹⁵ B. Meadows,³ J. R. T. de Mello Neto,¹ D. Mihalcea,⁷ R. H. Milburn,¹⁷
J. M. de Miranda,¹ A. Napier,¹⁷ A. Nguyen,⁷ A. B. d'Oliveira,^{3,12} K. O'Shaughnessy,²
K. C. Peng,⁶ L. P. Perera,³ M. V. Purohit,¹³ B. Quinn,⁹ S. Radeztsky,¹⁸ A. Rafatian,⁹
N. W. Reay,⁷ J. J. Reidy,⁹ A. C. dos Reis,¹ H. A. Rubin,⁶ D. A. Sanders,⁹ A. K. S. Santha,³
A. F. S. Santoro,¹ A. J. Schwartz,¹¹ M. Sheaff,^{4,18} R. A. Sidwell,⁷ A. J. Slaughter,¹⁹
M. D. Sokoloff,³ J. Solano,¹ N. R. Stanton,⁷ K. Stenson,¹⁸ D. J. Summers,⁹ S. Takach,¹⁹
K. Thorne,⁵ A. K. Tripathi,¹⁰ S. Watanabe,¹⁸ R. Weiss-Babai,¹⁵ J. Wiener,¹¹ N. Witchey,⁷
E. Wolin,¹⁹ D. Yi,⁹ S. Yoshida,⁷ R. Zaliznyak,¹⁴ and C. Zhang⁷

(Fermilab E791 Collaboration)

¹*Centro Brasileiro de Pesquisas Físicas, Rio de Janeiro, Brazil*

²*University of California, Santa Cruz, CA 95064*

³*University of Cincinnati, Cincinnati, OH 45221*

⁴*CINVESTAV, Mexico*

⁵*Fermilab, Batavia, IL 60510*

⁶*Illinois Institute of Technology, Chicago, IL 60616*

⁷*Kansas State University, Manhattan, KS 66506*

⁸*University of Massachusetts, Amherst, MA 01003*

⁹*University of Mississippi-Oxford, University, MS 38677*

¹⁰*The Ohio State University, Columbus, OH 43210*

¹¹*Princeton University, Princeton, NJ 08544*

¹²*Universidad Autonoma de Puebla, Mexico*

¹³*University of South Carolina, Columbia, SC 29208*

¹⁴*Stanford University, Stanford, CA 94305*

¹⁵*Tel Aviv University, Tel Aviv, Israel*

¹⁶*317 Belsize Drive, Toronto, Canada*

¹⁷*Tufts University, Medford, MA 02155*

¹⁸*University of Wisconsin, Madison, WI 53706*

¹⁹*Yale University, New Haven, CT 06511*

(March 26, 2018)

Abstract

We present a measurement of the form-factor ratios $r_V = V(0)/A_1(0)$ and $r_2 = A_2(0)/A_1(0)$ for the decay $D^+ \rightarrow \bar{K}^{*0} e^+ \nu_e$. The measurement is based on a signal of approximately 3000 $D^+ \rightarrow \bar{K}^{*0} e^+ \nu_e$, $\bar{K}^{*0} \rightarrow K^- \pi^+$ decays re-

constructed in data from charm hadroproduction experiment E791 at Fermi-lab. The results are $r_V = 1.84 \pm 0.11 \pm 0.08$ and $r_2 = 0.71 \pm 0.08 \pm 0.09$.

PACS numbers: 13.20.Fc,14.40.Lb

Semileptonic charm decays are useful for probing the dynamics of hadronic currents because Cabibbo-Kobayashi-Maskawa (CKM) weak mixing matrix elements for the charm sector are well known from unitarity constraints. Form factors are Lorentz-invariant functions of q^2 , the square of the virtual W mass in the decay, that describe how strong interactions modify the underlying weak decay [1]. Form factor measurements in semileptonic decays test a variety of models and nonperturbative calculations. In addition, Heavy Quark Effective Theory [2] relates form factors in semileptonic charm decays to those in bottom decays (at the same four-velocity transfer), which are needed to extract the weak mixing matrix elements $|V_{ub}|$ and $|V_{cb}|$ from semileptonic bottom decays. The vector form factor $V(q^2)$ and the axial-vector form factors $A_1(q^2)$ and $A_2(q^2)$ are relevant to the decay $D^+ \rightarrow \bar{K}^{*0} e^+ \nu_e$.

Using data from charm hadroproduction experiment E791 at Fermilab, we reconstruct about 3000 $D^+ \rightarrow \bar{K}^{*0} e^+ \nu_e$ (and charge-conjugate) decays (three times the largest previous sample [3]) and use the observed multidimensional distribution of kinematic variables to extract the form factor ratios $r_V = V(0)/A_1(0)$ and $r_2 = A_2(0)/A_1(0)$. We assume the nearest-pole dominance model for the q^2 dependence of the form factors, $F(q^2) = F(0)/(1 - q^2/m_{pole}^2)$ where m_{pole} is the appropriate vector or axial-vector pole mass: $m_V = 2.1 \text{ GeV}/c^2$ or $m_A = 2.5 \text{ GeV}/c^2$ [4].

E791 is a hadroproduction experiment [5] that generated charm using a 500 GeV/c π^- beam incident on five thin targets (one platinum, four diamond) separated by gaps of about 13.6 mm. E791 ran with a loose transverse energy trigger and recorded 20×10^9 interactions during the 1991-92 Fermilab fixed-target run. The important features of the E791 spectrometer for this analysis are the tracking system (23 planes of silicon microstrip detectors, 45 planes of drift and proportional wire chambers, and two large-aperture dipole magnets), two threshold Čerenkov counters that provide good K/π separation over the momentum range 6 - 36 GeV/c, and a lead-liquid-scintillator electromagnetic calorimeter.

In each event, we search for a candidate decay vertex (secondary vertex) with unit charge made from three charged tracks, separated from the reconstructed production vertex (primary vertex) by at least $15\sigma_z$ where σ_z is the uncertainty in the longitudinal separation. The decay vertex is required to be at least one measurement error outside the nearest target material. One charged particle must be consistent with being an electron as determined by electromagnetic shower shape, the match between calorimeter energy and tracking momentum, and the match between calorimeter and tracking position measurements. Electron identification efficiency is about 70%, while the probability for a pion to be misidentified as an electron is only 1 - 2%. One of the two remaining charged particles must have a Čerenkov kaon signature. Kaon identification efficiency is about 65% in the momentum range 6 - 36 GeV/c and lower above this range. The probability for misidentifying a pion as a kaon is about 5% in the same momentum range and significantly lower above this range. Candidates consistent with being misidentified $D^+ \rightarrow K^- \pi^+ \pi^+$ decays are removed. If electron and kaon candidates are oppositely charged, the decay is a candidate for $D^+ \rightarrow \bar{K}^{*0} e^+ \nu_e$, $\bar{K}^{*0} \rightarrow K^- \pi^+$. We call them “right-sign” decays. If electron and kaon candidates have the same charge, the decay is classified as “wrong-sign”. The wrong-sign sample is used to model background in the right-sign sample. A clear excess of right-sign events compared to wrong-sign events is seen in the $K\pi$ invariant mass distribution at the \bar{K}^{*0} mass.

The final $K\pi e\nu_e$ sample (see Fig. 1) is optimized with a binary-decision-tree algorithm (CART [6]) that finds the set of “splits” in a set of single parameters or linear combinations

of parameters that best separates signal from background. We train CART using a subsample ($\approx 15\%$) of the right-sign candidates for signal and the wrong-sign candidates for background. CART selected a single cut involving a linear combination of four discrimination variables: (a) separation significance of the candidate decay vertex from target material, (b) distance of closest approach of the candidate D momentum vector to the primary vertex allowing for the maximum kinematically-allowed miss distance due to the unobserved neutrino, (c) product over candidate D decay tracks of the distance of closest approach of the track to the secondary vertex divided by the distance of closest approach to the primary vertex, where each distance is measured in units of measurement errors, and (d) separation significance between the production and decay vertices. This selection criterion halved the number of wrong-sign events in the signal region, and kept 75% of right-sign events.

Figure 1 shows mass distributions for the final right-sign (RS) and wrong-sign (WS) $K\pi e\nu_e$ candidates. The top left plot shows the distribution of M_{min} , the minimum $K\pi e\nu_e$ mass kinematically allowed by the D direction as determined from the measured K , π , and e momenta and the positions of the primary and secondary vertices, with a $0.75 < M(K\pi) < 1.05$ GeV/ c^2 cut for both the right-sign and wrong-sign events. The M_{min} distribution for true $D^+ \rightarrow K^-\pi^+e^+\nu_e$ events (with no detector smearing) would have a cusp at the D mass (1.869 GeV/ c^2). The bottom left plot in Fig. 1 shows the $M(K\pi)$ distribution for events with $1.6 < M_{min} < 2.0$ GeV/ c^2 . Of these, there are 3595 right-sign and 602 wrong-sign events with $0.85 < M(K\pi) < 0.94$ GeV/ c^2 (indicated by the vertical arrows in the figures), which are used to extract the form-factor ratios. The right-hand plot in Fig. 1 shows the difference between the right-sign and wrong-sign distributions. The net $K\pi$ signal is dominantly K^{*0} as can be seen from the superposed fit of the $M(K\pi)$ spectrum to a pure Breit-Wigner shape with the mass and width fixed to the known values of the K^{*0} resonance. There is an excess of events over that expected for a Breit-Wigner distribution in the region below the $M(K\pi)$ range used in the analysis. The assumption that wrong-sign events accurately model the size and shape of the right-sign background is addressed in the discussion of systematic uncertainties below.

The kinematic variables used in extracting the form factor ratios are the square of the invariant mass of the virtual W (q^2) and three angles. The polar angle θ_e , measured in the virtual W (or $e\nu$) rest frame, is the angle between the charged lepton and the direction opposite the K^{*0} . The polar angle θ_V , measured in the K^{*0} rest frame, is the angle between the K and the direction opposite the virtual W . The azimuthal angle χ is the angle between the momentum projections of the electron and K in the plane perpendicular to the K^{*0} direction in the D rest frame. To calculate these variables, the neutrino momentum is estimated up to a two-fold ambiguity from the D flight direction as determined by the measured positions of the D production and decay points, and the measured momenta of the charged decay products. Monte-Carlo simulation shows less kinematic variable smearing for the solution which results in the lower D momentum, so it is used.

We extract the form factors using an unbinned maximum-likelihood method that uses a Monte-Carlo simulation in the evaluation of the likelihood function [7,8]. The production physics and detector response are simulated for an event set that is passed through the same analysis chain as the data. The simulated events are generated with specified form-factor ratios (0.82 for r_2 , 2.00 for r_V) [9]. The likelihood of the data sample is calculated, for any given set of theoretical parameters, by computing the density of Monte-Carlo events

in a specified volume around each data point, where the simulated events are distributed according to the theoretical parameters under consideration. To avoid generating separate Monte-Carlo samples for every set of theoretical parameters considered in the fit, a single Monte-Carlo sample is reweighted so that the weighted events give the correct density about each data point. As long as the Monte Carlo accurately simulates both the charm production process and the detector response, acceptance and smearing effects are automatically incorporated into the fit. The wrong sign candidates are used to incorporate backgrounds into the fit with a similar technique. We developed a second method to extract form factors that keeps both neutrino momentum solutions and we use it as a check. To account for the wrong solution, we use Monte Carlo simulation to determine a feedthrough matrix that gives the probability that an event appearing in one region of the space of measured kinematic variables would appear in another region when the other solution for neutrino momentum is used. This matrix and the observed distribution of data events (both solutions) determine the fraction of data events that correspond to the correct neutrino-momentum solution in each region of kinematic-variable space. Each fraction is then used in a binned maximum likelihood fit, with background modeled as in the first method.

The first fitting technique gives $r_V = 1.84 \pm 0.11 \pm 0.08$ and $r_2 = 0.71 \pm 0.08 \pm 0.09$ with a correlation coefficient of -0.13 . The first error is statistical, and the second systematic (discussed below). The above results have been corrected for biases of less than 10% due to the technique, determined from fitting Monte-Carlo samples with known form-factor ratios. The second fitting technique gives $r_V = 1.78 \pm 0.12$ and $r_2 = 0.68 \pm 0.07$, where the errors are statistical only. The Monte Carlo indicates no correction for bias is required. The results from the second fitting technique are consistent with the first.

Possible sources of systematic uncertainties were considered and the most important are summarized in Table I. To estimate the effects of possible inaccuracies in the Monte-Carlo simulation of the detector response, 15 different sets of selection criteria were generated using different training samples for CART. The spread in the resulting form-factor ratios gives our estimate of this systematic uncertainty [10]. We estimate the uncertainty due to our modeling of the background by varying our assumptions about the amount and the distribution of the background in the four-dimensional kinematic variable space. We have determined that $D^{*+} \rightarrow D^0\pi^+$, $D^0 \rightarrow K^-e^+\nu_e$, and $D^+ \rightarrow \bar{K}^{*0}\pi^0e^+\nu_e$ modes do not contribute significantly to the background in the signal region. Other sources of systematic uncertainty are the limited size of the Monte-Carlo sample and uncertainties in charged-particle identification efficiency. The contributions from each source are added in quadrature giving the total error of 0.08 and 0.09 for r_V and r_2 , respectively.

Figure 2 shows the projections of the kinematic variables $\cos\theta_V$, $\cos\theta_e$, and χ for data and for Monte-Carlo events that have been weighted according to the best fit values for the form-factor ratios. To reveal the correlations between the observed kinematic variables, we show plots for each variable for two ranges of a second variable. The confidence level for the consistency of the Monte Carlo and data projections is shown on each plot.

Throughout, we have assumed the nearest pole dominance q^2 dependence $F(q^2) = F(0)/(1-q^2/m_{A,V}^2)$ which can be approximated by a form linear in q^2 , $F(q^2) = F(0)(1+\rho^2q^2)$. This is a valid approximation in the accessible q^2 range (0 - 0.947 GeV²/c⁴). We perform a three-parameter fit for the slope ρ_A^2 and the form-factor ratios r_V and r_2 (fixing $\rho_A^2/\rho_V^2 = m_V^2/m_A^2$). The result for r_V is 1.88 ± 0.11 , which is close to the two-parameter

fit. The results for r_2 and ρ_A^2 are strongly anticorrelated, so the statistical uncertainty on these two parameters is large. The result for r_2 is $0.98_{-0.15}^{+0.14}$, which is about two standard deviations higher than the result of the two-parameter fit. The result for ρ_A^2 is $-0.06_{-0.09}^{+0.10}$ $\text{GeV}^{-2}c^4$, which is about two standard deviations lower than the theoretical expectation $\rho_A^2 = 1/m_A^2 = 0.16 \text{ GeV}^{-2}c^4$.

Table II compares the form-factor ratios measured by this experiment and previously published results. All measurements are in accord. Using the world averages for $B(D^+ \rightarrow \bar{K}^{*0} e^+ \nu_e)$ and the D^+ lifetime [4], we extract the values of the form factors A_1 , A_2 , and V at $q^2 = 0$ and at $q^2 = q_{max}^2$. We account for both the finite width of the \bar{K}^{*0} and the correlation between the measured form-factor ratios [12]. Table III compares these results with predictions from Lattice Gauge calculations [13–16] and a quark model calculation [17] based on Heavy Quark Effective Theory. The former are in fair agreement with the experimental results, while the latter is not, in particular for $A_2(q_{max}^2)$.

In summary, we have used a sample of 3000 signal events to extract the form-factor ratios in the decay $D^+ \rightarrow \bar{K}^{*0} e^+ \nu_e$: $r_V = 1.84 \pm 0.11 \pm 0.08$ and $r_2 = 0.71 \pm 0.08 \pm 0.09$. The combined statistical and systematic uncertainties are a bit less than half the best previous measurement. The form-factor ratios are important for improving our understanding of the dynamics of hadronic currents and might improve our ability to extract CKM matrix elements from B semileptonic decays.

We thank the staffs of Fermilab and all the participating institutions for assistance. This work was supported by the Brazilian Conselho Nacional de Desenvolvimento Científico e Tecnológico, CONACyT (Mexico), the Israeli Academy of Sciences and Humanities, the U.S. Dept. of Energy, the U.S.-Israel Binational Science Foundation, and the U.S. National Science Foundation. Fermilab is operated by the Universities Research Association under contract with the U.S. Dept. of Energy.

REFERENCES

- [1] J.D. Richman and P.R. Burchat, *Rev. Mod. Phys.* **67**, 893 (1995).
- [2] N. Isgur and M.B. Wise, *Phys. Rev. D* **42**, 2388 (1990).
- [3] P.L. Frabetti *et al.*, *Phys. Lett. B* **307**, 262 (1993).
- [4] *Review of Particle Physics*, *Phys. Rev. D* **54** (1996).
- [5] J.A. Appel, *Ann. Rev. Nucl. Part. Sci.* **42**, 367 (1992); D.J. Summers *et al.*, XXVII Rencontre de Moriond, Les Arcs, France (15-22 March 1992) 417.
- [6] L. Brieman *et al.*, *Classification and Regression Trees* (Chapman and Hall, New York, 1984).
- [7] D.M. Schmidt, R.J. Morrison, and M.S. Witherell, *Nucl. Instrum. Methods A* **328**, 547 (1993).
- [8] J.C. Anjos *et al.*, *Phys. Rev. Lett.* **65**, 2630 (1990).
- [9] For the general expression of the differential decay rate in terms of kinematic variables and form factors, see Eqs. 113, 115, and 116 in [1], or Eqs. 2 and 3 on p. 482 in [4]. In ref. [4] $\cos\theta_e$ is defined as the angle between the charged lepton and the vector meson direction.
- [10] We remove the contribution to the spread in form-factor ratios due to the partial statistical independence of the 15 samples, determined from Monte Carlo.
- [11] K. Kodama *et al.*, *Phys. Lett. B* **274**, 246 (1992).
- [12] A. Ryd, private communication, using software originally written by R. Culbertson.
- [13] C.R. Allton *et al.*, *Phys. Lett. B* **345**, 513 (1995).
- [14] S. Gusken *et al.*, *Nucl. Phys. Proc. Suppl.* **47**, 485 (1996).
- [15] J. Nieves *et al.*, *Nucl. Phys. Proc. Suppl.* **42**, 431 (1995).
- [16] A. Abada *et al.*, *Nucl. Phys. B* **416**, 675 (1994).
- [17] D. Scora and N. Isgur, *Phys. Rev. D* **52**, 2783 (1995).

TABLES

TABLE I. Contributions to the systematic uncertainty.

Source of Uncertainty	σ_{r_V}	σ_{r_2}
Simulation of detector effects	0.03	0.03
Monte Carlo volume size	0.04	0.04
Background volume size	0.04	0.05
Amount of background	0.02	0.05
Particle identification efficiency	0.05	0.01
Fitting technique	0.01	0.01
Total Estimate	0.08	0.09

TABLE II. Results of this analysis (E791) and comparison with other experiments. The approximate number of signal events and the lepton type used in each analysis is also listed.

Experiment	$r_V = V(0)/A_1(0)$	$r_2 = A_2(0)/A_1(0)$	Events
E791	$1.84 \pm 0.11 \pm 0.08$	$0.71 \pm 0.08 \pm 0.09$	3000 (e)
E687 [3]	$1.74 \pm 0.27 \pm 0.28$	$0.78 \pm 0.18 \pm 0.10$	900 (μ)
E653 [11]	$2.00^{+0.34}_{-0.32} \pm 0.16$	$0.82^{+0.22}_{-0.23} \pm 0.11$	300 (μ)
E691 [8]	$2.0 \pm 0.6 \pm 0.3$	$0.0 \pm 0.5 \pm 0.2$	200 (e)

TABLE III. Form factors extracted from the measured ratios r_V and r_2 , and several theoretical predictions.

Group	$A_1(0)$	$A_2(0)$	$V(0)$
E791	0.58 ± 0.03	0.41 ± 0.06	1.06 ± 0.09
APE [13]	0.67 ± 0.11	0.49 ± 0.34	1.08 ± 0.22
Wuppertal [14]	$0.61^{+0.11}_{-0.09}$	$0.83^{+0.23}_{-0.22}$	$1.34^{+0.31}_{-0.28}$
UKQCD [15]	$0.70^{+0.07}_{-0.10}$	$0.66^{+0.10}_{-0.15}$	$1.01^{+0.30}_{-0.13}$
ELC [16]	0.64 ± 0.16	0.41 ± 0.28	0.86 ± 0.24
	$A_1(q_{max}^2)$	$A_2(q_{max}^2)$	$V(q_{max}^2)$
E791	0.68 ± 0.04	0.48 ± 0.08	1.35 ± 0.12
ISGW2 [17]	0.70	0.94	1.52

FIGURES

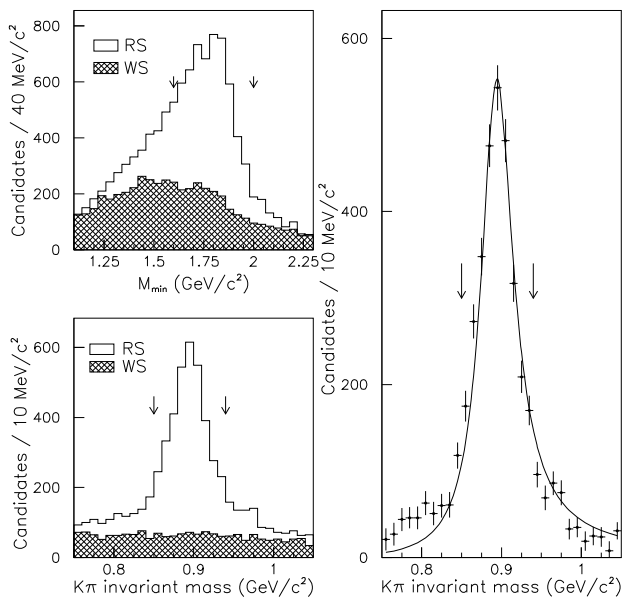


FIG. 1. Final sample of $D^+ \rightarrow \bar{K}^{*0} e^+ \nu_e$, $\bar{K}^{*0} \rightarrow K^- \pi^+$ candidates. The distributions are described in the text.

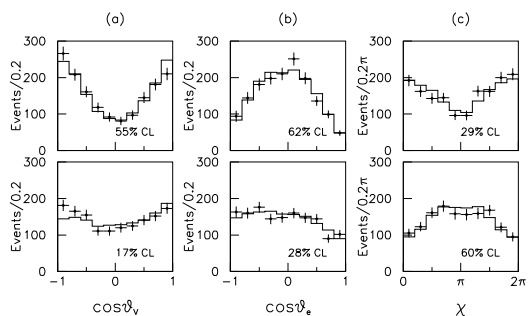


FIG. 2. Data distributions (black dots with errors) overlaid with Monte Carlo (histogram) for (a) $\cos \theta_V$ for $q^2/q_{max}^2 \leq 0.5$ (top) and $q^2/q_{max}^2 > 0.5$ (bottom), (b) $\cos \theta_e$ for $q^2/q_{max}^2 \leq 0.5$ (top) and $q^2/q_{max}^2 > 0.5$ (bottom), (c) χ for $\cos \theta_V \leq 0$ (top) and $\cos \theta_V > 0$ (bottom). The Monte-Carlo events are weighted according to the best-fit values of the form-factor ratios.